Differences in Photophysical Properties and Photochemistry of Ru(II)-Terpyridine Complexes of CH_3CN and Pyridine

Marilyn N. Dunbar†, Sean J. Steinke†, Eric J. Piechota, and Claudia Turro*

Department of Chemistry and Biochemistry, The Ohio State University, Columbus, OH 43210

Abstract. A series of 22 Ru(II) complexes of the type $[Ru(tpy)(L)(L')]^{n+}$, where tpy is the tridentate ligand 2,2';6,2"-terpyridine, L represents bidentate ligands with varying electron donating ability, and L' is acetonitrile (**1a – 11a**) or pyridine (**1b** – **11b**), were investigated. The dissociation of acetonitrile occurs from the ^{3}MLCT state in **1a** – **11a**, such that it does not require the population of a ^{3}LF state. Electrochemistry and spectroscopic data demonstrate that the ground states of these series do not differ significantly. Franck-Condon line-shape analysis of 77 K emission data shows no significant differences between the emitting ^{3}MLCT states in both series. Arrhenius analysis of the temperature dependence of ^{3}MLCT lifetimes shows that the energy barrier (E_a) to thermally populating a ^{3}LF state from a lower energy ^{3}MLCT state is significantly higher in the pyridine than the CH_3CN series, consistent with the photostability of complexes **1b** – **11b** which do not undergo pyridine photodissociation under our experimental conditions. Importantly, these results demonstrate that ligand photodissociation of pyridine in **1b** – **11b** does not take place directly from the ^{3}MLCT state, as is the case for **1a – 11a**. These findings have potential impact on the rational design of complexes for a number of applications, including photochemotherapy, dye-sensitized solar cells, and photocatalysis.

---

† These authors contributed equally to this work.

*Corresponding Author: C. Turro: turro.1@osu.edu

Introduction.

Ruthenium(II) polypyridyl complexes have been investigated for applications in areas that include photochemotherapy (PCT), photodynamic therapy (PDT), photocatalysis, dye-sensitized solar cells, and sensing, among many others.[1–6] These complexes possess strong electronic absorption in the visible region, long-lived excited states, and highly tunable properties through the synthetic modification of the ligands, which provide them with valuable versatility. The absorption of light by Ru(II) polypyridyl complexes results in the population of a singlet metal-to-ligand charge transfer (^{1}MLCT) excited state that undergoes rapid (<50 fs) intersystem crossing to the corresponding ^{3}MLCT state.[7,8] The unimolecular decay from the ^{3}MLCT excited state occurs through a number of competing pathways, including nonradiative and radiative decay directly to the singlet ground state, ^{1}GS, with rate constants k_{nr} and k_r, respectively. The deactivation of ^{3}MLCT states in Ru(II) complexes may also take place through the dissociation of a ligand to generate a photoproduct and/or the thermal population of a triplet ligand field (^{3}LF) state, which typically exhibits efficient thermal deactivation to the ^{1}GS.[9–13] Understanding the molecular properties that influence these various relaxation pathways and the rates of excited state deactivation in Ru(II) complexes is critical for the rational design of new systems to improve their particular function in each application.

The decay of an excited state back to the ground state, excluding deactivation through bond-breaking, is characterized by small displacements in bond lengths and angles, as well as reorganization of solvent molecules around the excited complex in the solution phase. These structural changes result in differences in equilibrium geometries between the ground and excited states. This nuclear displacement affects the Franck-Condon overlap of excited and ground states and impacts the rate of excited state decay. The ^{3}MLCT excited state lifetime is also affected by the energy difference between the excited and ground state, E_{00}, because k_{nr} increases as E_{00} decreases, as dictated by the energy gap law.[14–16] This effect is exemplified by two homoleptic Ru(II) complexes bearing the tridentate ligand 2,6-di(quinolin-8-yl)pyridine (dqp) with a substituent, R, at the 4-position of the central pyridine ring.[17] When R = –CO_2Et, the energy of the

^{3}MLCT emissive state is 1.88 eV with a lifetime, τ, of 11.2 μs at 80 K, while the complex with R = –NH_2, $[Ru(dqpNH_2)_2]^{2+}$, was measured to have E_{00} = 1.71 eV and τ = 2.7 μs under similar conditions. The shorter lifetime measured for $[Ru(dqpNH_2)_2]^{2+}$ is consistent with the energy gap law. Excited state photophysics governed by the energy gap law are important to consider when designing transition metal complexes because it can place limitations on photoreactivity. For example, low-energy absorption is desirable in ruthenium(II) complexes intended for PDT applications, such that E_{00} is relatively low. In addition, bimolecular energy transfer to produce cytotoxic $^1O_2$ following visible light excitation is required. The lower energy triplet excited state results in shorter lifetimes, reducing the efficiency for $^1O_2$ production, which can make some complexes less desirable for PDT.[18–20]

Ruthenium(II) complexes that undergo photoinduced ligand exchange for photochemotherapy (PCT) applications are stable in solution prior to irradiation and release a biologically-active molecule following the absorption of light. The Turro group, among others, has reported model Ru(II) complexes that undergo photoinduced ligand exchange, including those with nitrile, pyridyl, and thioether groups coordinated to the metal.[21–25] Additionally, the photoinduced release of clinically approved therapeutic agents from Ru(II) complexes has been demonstrated.[26–30] The generally accepted mechanism of photoinduced ligand dissociation relies on the thermal population of a ^{3}LF state from the lowest-energy ^{3}MLCT state. This ^{3}LF state is Ru–L(dσ*) in nature, such that its population weakens the Ru-L bond, resulting in the dissociation of the monodentate ligand.[31,32] An important factor that affects the population of the ^{3}LF state is the activation barrier, E_a, which is dependent on the relative energies of the ^{3}MLCT and ^{3}LF states, as well as the nuclear displacement and electronic coupling between the ^{3}MLCT and ^{3}LF potential energy surfaces. It is expected that complexes that feature smaller energy gaps and lower activation barriers should exhibit higher efficiencies for ligand exchange, however, recent work has shown that this is not always the case. In particular, the Turro group demonstrated that a series of complexes with the formula $[Ru(tpy)(L)(CH_3CN)]^{n+}$ (tpy = 2,2':6,2"-terpyridine, L = a series of bidentate ligands of varying electron donating ability), complexes **1a** – **11a** in Figure 1, undergo

CH_3CN photosubstitution following visible light irradiation.[33,34] The complexes in this series possess lowest energy ^{3}MLCT states with lifetimes that increase as the energy of the ^{3}MLCT state decreases, a trend that is the reverse that which is expected from the energy gap law.[33,34] It was also shown that the photosubstitution of the CH_3CN ligand from **1a** – **11a** occurs with greater efficiency as the barrier to populating the ^{3}LF state from the ^{3}MLCT state increased, analogous to the pattern observed for excited state lifetimes.[35] Combined with DFT calculations, it was concluded that ligand dissociation occurs directly from the ^{3}MLCT state in complexes **1a** – **11a**, contrary to the currently accepted mechanism of photosubstitution in Ru(II) polypyridyl complexes which require the population of the Ru–L(σ*) ^{3}LF state.

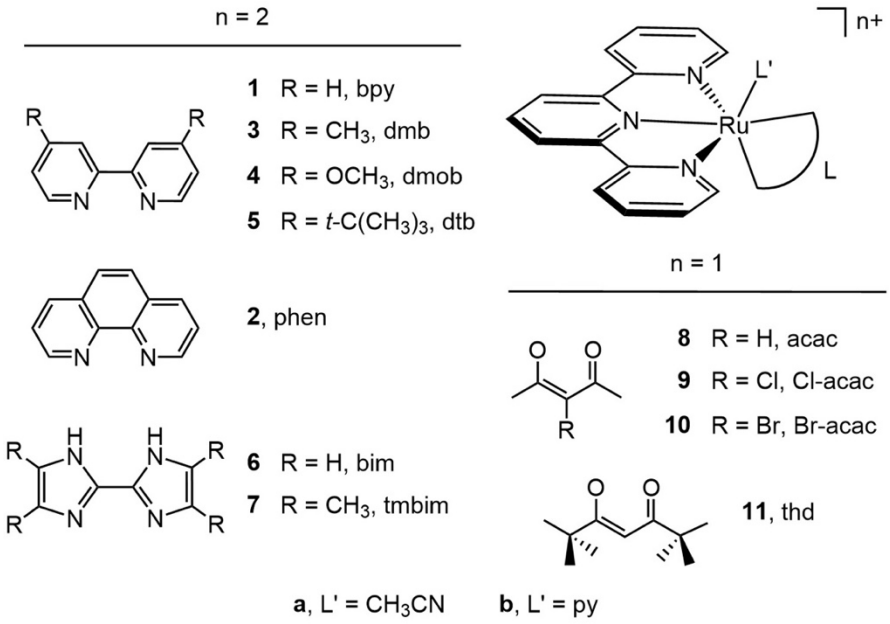

Figure 1. Schematic representation of the molecular structures of **1a** – **11a** (L' = CH_3CN) and **1b** – **11b** (L' = py).

The photodissociation of a ligand from a Ru(II) polypyridyl complex is known to depend on the identity of the leaving ligand. Generally, pyridine ligands form a strong σ-bond to transition metals, whereas the less basic CH_3CN ligand exhibits weak σ-bonding and relies on π-

backbonding when coordinating to ruthenium(II).[36,37] Owing to the strong Ru-N σ-bond, pyridine complexes undergo ligand exchange with lower quantum yields than the corresponding CH_3CN complexes under similar experimental conditions.[22–24,38] In order for pyridine photodissociation to take place efficiently, steric bulk is required to lower the energy of the ^{3}LF below the ^{3}MLCT state. This is evident in $[Ru(tpy)(6,6'\text{-}Me_2bpy)(py)]^{2+}$ (Φ_{500} = 0.16) and $[Ru(tpy)(biq)(py)]^{2+}$ (Φ_{500} = 0.033) in CH_3CN, where the incorporation of steric bulk results in distortions around the pseudo-octahedral coordination environment around the Ru(II) center compared to $[Ru(tpy)(bpy)(py)]^{2+}$, lowering the energy of the e_g-type(σ*) orbital set and, consequently, the ^{3}LF state.[23] In addition, the identity of the monodentate ligand influences a number of electronic properties of the triplet excited states of Ru(II) complexes, including the orbital contributions and energies, which have a significant impact on the photophysical properties. The present work focuses on the investigation of the role that the acetonitrile ligand plays in the unexpected photophysical behavior previously reported for **1a** – **11a**, as well as a comparison to the analogous pyridine complexes **1b** – **11b**, which were synthesized, and their ground and excited states properties were characterized (Figure 1).

Experimental.

Materials. All chemical and solvents were used as received and were of reagent grade for synthetic use and instrumental analysis except where otherwise noted. Acetonitrile, acetone, diethyl ether, and methanol (MeOH) were purchased from Fisher Scientific, ethanol (EtOH, 200 proof) was obtained from Decon Laboratories, and ammonium hexafluorophosphate was purchased from Oakwood Chemical. Tetrabutylammonium hexafluorophosphate ($TBAPF_6$), pyridine (py), and $(CD_3)_2CO$ were purchased from Sigma Aldrich. The ligands 4,4'-dimethoxy-2,2'-bipyridine (dmob), 4,4'-di-*tert*-butyl-2,2'-bipyridine (dtb), 2,2'-biimidazole (bim), and 2,2'-bis(4,5-dimethylimidazole) (tmbim) were all purchased from Sigma Aldrich. The synthetic precursors $[Ru(tpy)(dmob)Cl](PF_6)$, $[Ru(tpy)(dtb)Cl](PF_6)$, $[Ru(tpy)(bim)Cl](PF_6)$, and $[Ru(tpy)(tmbim)Cl](PF_6)$, as well as complexes **1a** – **11a**, **1b** – **3b**, and **8b** – **11b** were synthesized

according to previously published procedures.[23,33,38–40] All reactions were performed under a nitrogen atmosphere. The CH_3CN used in electrochemical measurements was purified through distillation over CaH_2 and acetone used in transient absorption experiments was purchased as spectroscopic grade from Sigma-Aldrich.

[Ru(tpy)(dmob)(py)](PF$_6$)$_2$ (4b). [Ru(tpy)(dmob)Cl](PF$_6$) (0.038 g, 0.0.052 mmol) was dissolved in 15 mL EtOH/H_2O (1:1, v:v) in a 50 mL round bottom flask. An excess of pyridine (~3 mL) was added to the reaction mixture, the flask was heated to reflux, and the reaction was allowed to reflux overnight in the dark. After cooling, the solution was concentrated by rotary evaporation and added to a concentrated solution of NH_4PF_6 in H_2O. The resulting precipitate was collected through vacuum filtration, washed thrice with 20 mL aliquots of H_2O, and dried with diethyl ether to afford **4b** as a maroon solid (0.042 g, 88% yield). ^{1}H NMR (600 MHz, $(CD_3)_2CO$, Figure S1): δ 8.83 (d, 2H, J = 8.1 Hz), 8.74 (d, 2H, J = 7.9 Hz), 8.72 (d, 1H, J = 6.5 Hz), 8.56 (d, 1H, J = 2.8 Hz), 8.34 (t, 1H, J = 8.2 Hz), 8.29 (d, 1H, J = 2.7 Hz), 8.20 (d, 2H, J = 4.8 Hz), 8.18 (d, 2H, J = 7.8 Hz), 8.01 (d, 2H, J = 6.5 Hz), 7.89 (t, 1H, J = 7.6 Hz), 7.62 (m, 3H), 7.34 (d, 2H, J = 7.0 Hz), 7.31 (d, 1H, J = 6.5 Hz), 6.79 (dd, 1H, J = 3.8, 2.9 Hz), 4.23 (s, 3H), 3.92 (s, 3H). ESI-MS(+): [M – $(PF_6)_2]^{2+}$ *m/z* = 315.065 (calc. *m/z* = 315.066), [M – $PF_6]^+$ *m/z* = 775.095 (calc. *m/z* = 775.095).

[Ru(tpy)(dtb)(py)](PF$_6$)$_2$ (5b). This complex was synthesized in a procedure similar to **4b** dissolving [Ru(tpy)(dtb)Cl](PF$_6$) (0.033 g, 0.043 mmol) in 15 mL EtOH/H_2O (1:1, v:v) to yield **5b** as a dark red solid (0.030 g, 72% yield). ^{1}H NMR (600 MHz, $(CD_3)_2CO$, Figure S2): δ9.03 (d, 1H, J = 2.0 Hz), 8.86 (m, 3H), 8.78 (d, 1H, J = 1.9 Hz), 8.76 (d, 2H, J = 8.1 Hz), 8.38 (t, 1H, J = 8.1 Hz), 8.19 (td, 2H, J = 8.0, 1.4 Hz), 8.09 (d, 2H, J = 5.6 Hz), 8.04 (m, 3H), 7.91 (t, 1H, J = 7.6 Hz), 7.58 (t, 2H, J = 6.6 Hz), 7.48 (d, 1H, J = 6.2 Hz), 7.36 (t, 2H, J = 6.6 Hz), 7.23 (dd, 1H, J = 6.3, 2.2 Hz), 1.57 (s, 9H), 1.26 (s, 9H). ESI-MS(+):[M – $(PF_6)_2]^{2+}$ *m/z* = 315.065 (calc. *m/z* = 315.066), [M – $PF_6]^+$ *m/z* = 827.198 (calc. *m/z* = 827.201).

[Ru(tpy)(bim)(py)](PF$_6$)$_2$ (6b). This complex was synthesized in a procedure similar to that describe for **4b** using [Ru(tpy)(bim)Cl](PF$_6$) (0.044 g, 0.068 mmol) in 1:1 EtOH/H_2O (15 mL) to

yield **6b** (0.025 g, 43% yield). ^{1}H NMR (600 MHz, $(CD_3)_2CO$, Figure S3): δ 8.79 (d, 2H, J = 8.2 Hz), 8.68 (d, 2H, J = 7.9 Hz), 8.28 (t, 1H, J = 8.2 Hz), 8.24 (d, 2H, J = 5.5 Hz), 8.20 (d, 2H, J = 5.4 Hz), 8.12 (t, 2H, J = 7.9 Hz), 7.99 (d, 1H, J = 1.4 Hz), 7.84 (t, 1H, J = 7.7 Hz), 7.80 (d, 1H, J = 1.5 Hz), 7.60 (t, 2H, J = 6.7 Hz), 7.33 (t, 2H, J = 7.1 Hz), 7.18 (d, 1H, J = 1.5 Hz), 6.23 (d, 1H, J = 1.5). ESI-MS(+): $[M - PF_6]^+$ *m/z* = 693.063 (calc. *m/z* = 693.065).

[**Ru(tpy)(tmbim)(py)](PF$_6$)$_2$ (**7b**). [Ru(tpy)(tmbim)Cl](PF$_6$) (0.049 g, 0.066 mmol) was dissolved in 20 mL EtOH/H_2O (1:1 v:v) in a 50 mL round bottom flask. An excess of pyridine (~3 mL) was added to the reaction mixture, the flask was heated to reflux, and the solution was allowed to reflux overnight. After cooling, the mixture was reduced to one quarter of its original volume by rotary evaporation and a small amount of NH_4PF_6 was added to precipitate **7b**. The solid was collected by vacuum filtration, rinsed with H_2O (3 x 20 mL), followed by diethyl ether (3 x 20 mL), and then redissolved from the glass filter frit with acetone. The filtrate was centrifuged to remove any excess NH_4PF_6 and the supernatant was concentrated through rotary evaporation, reprecipitated by adding the solution to diethyl ether, and collected on a glass fritted filter again to yield **7b** (0.041 g, 66% yield). ^{1}H NMR (600 MHz, $(CD_3)_2CO$, Figure S4): δ 8.74 (d, 2H, J = 8.1 Hz), 8.71 (d, 2H, J = 8.1 Hz), 8.32 (d, 2H, J = 5.4 Hz), 8.19 (t, 3H, J = 8.3), 7.89 (d, 2H, J = 5.8 Hz), 7.79 (t, 1H, J = 7.8), 7.70 (t, 2H, J = 6.5 Hz), 7.22 (t, 2H, J = 7.3 Hz), 2.43 (s, 3H), 1.90 (s, 3H), 1.72 (s, 3H), 1.01 (s, 3H). ESI-MS(+): $[M - (PF_6)_2]^{2+}$ *m/z* = 302.082 (calc. *m/z* = 302.082), $[M - PF_6]^+$ *m/z* = 749.126 (calc. *m/z* = 749.128).

Instrumentation and Methods. ^{1}H NMR spectra were collected using a Bruker Avance III HD Ascend 600 MHz spectrometer, electrospray ionization (ESI) mass spectrometry experiments were performed using a Bruker microTOF mass spectrometer, and electrochemistry was recorded on a BASi Epsilon Eclipse electrochemical analyzer (Bioanalytical Systems, Inc.). ^{1}H NMR spectra were collected in $(CD_3)_2CO$ and all chemical shifts were referenced to the residual protonated solvent peak.[41] ESI mass spectrometry data was collected in positive mode using MeOH as the eluent and referenced to a sodium trifluoroacetate standard. Cyclic voltammograms were obtained

under an inert atmosphere with a three-electrode cell utilizing a glassy carbon working electrode, a Pt wire auxiliary electrode, and a saturated Ag/AgCl (3 M NaCl) reference electrode. Samples were dissolved in CH_3CN containing 0.1 M $TBAPF_6$ as an electrolyte, data were collected at a scan rate of 100 mV s^{-1}, and ferrocene (Fc) was added at the end of each experiment as an internal reference ($Fc^{+/0}$ = +0.44 vs Ag/AgCl in CH_3CN).[42]

Steady state electronic absorption spectra were collected on an Agilent Cary 8453 or 8454 diode array spectrophotometer using 1x1 cm quartz cuvettes with fused Kontes tops. Emission data for Franck–Condon line-shape analysis were collected using a Fluorolog-3 fluorimeter equipped with a Horiba Synapse 354308 CCD. Room temperature emission lifetimes for **1b** – **5b** were collected on a time-correlated single-photon counting instrument, Horiba fluorolog-3, equipped with a Hamamatsu R928 photomultiplier tube detector. Samples were excited with a Horiba Scientific N-510L NanoLED pulsed diode light source at a wavelength of 510 ± 10 nm with a pulse duration of < 200 ps. The luminescence lifetimes of **6b** – **11b** were collected on the ns laser system described herein and excited with a 500 nm pulse.

Nanosecond transient absorption (nsTA) experiments were performed using an LP980 spectrometer system (Edinburgh Instruments) equipped with a 150 W Xe arc lamp (Osram) as a probe beam, a PMT and digital oscilloscope (Tektrnoix MDO3022, 200 MHz, 2.5 GS/s) for single-wavelength kinetic traces, and an intensified CCD (ICCD, Andor iStar) for spectral measurements. Samples were excited by the output from a basiScan tunable Optical Parametric Oscillator (OPO, SpectraPhysics) pumped by a frequency-tripled (355 nm) Quanta-Ray INDI Nd:YAG laser (SpectraPhysics, fwhm ~6 ns, 10 Hz repetition rate). Nanosecond transient absorption (nsTA) data at room temperature and variable temperatures were obtained in spectroscopic grade acetone in a 1x1 cm quartz cuvette with a fused Kontes top and were sparged for 20 min with Ar prior to measurement to remove dissolved O_2. The absorption spectrum of each sample was obtained post-experiment for comparison to the initial absorption spectrum to ensure no sample degradation had occurred (Figures S5 – S6). Single-wavelength kinetic traces were fit to monoexponential decays when $\tau > 30$ ns and a reconvolution of the instrument response function (~6 ns) was used when τ

< 30 ns available in the L900 software (Edinburgh Instruments). Samples were prepared in acetone with an absorbance of 0.2 – 0.5 at the excitation wavelength and sparged with Ar for 20 minutes prior to data acquisition. For complexes **1b** – **5b**, emission lifetimes were collected at the emission maxima with a bandwidth of 8 nm and were fit to a monoexponential function using a reconvolution fit in the L900 software (Edinburgh Instruments) which accounts for the TCSPC instrument response function (~500 ps). For complexes **6b** – **11b**, lifetimes were determined from single-wavelength kinetic traces of excited state absorption features and fit to a monoexponential function.

Temperature control for the measurement of the temperature dependence of the excited state lifetimes was achieved with a CoolSpeK UV USP-203-B cryostat (UNISOKU Scientific Instruments). For the temperature dependence experiments, the cryostat was heated to +100 °C with a positive flow of Ar through the empty sample chamber for one hour to remove atmospheric water. The chamber was then sealed, cooled to room temperature, and the sample of interest was quickly placed in the sample chamber and resealed to maintain an Ar environment. The cryostat was then cooled to –100 °C with liquid N_2 and maintained at that temperature for one hour prior to the first measurement. Each temperature at which a sample was analyzed above –100 °C was maintained for 15 min prior to measurement to ensure sample equilibration and data was acquired in three separate trials over the entire temperature range of analysis.

Electronic Structure Calculations. Spin restricted and unrestricted density functional theory (DFT) calculations were performed using the Gaussian09 program package.[43] Geometry optimizations and vibrational frequency and molecular orbital calculations were performed with the SDD[44] basis set on Ru and the TZVP[45] basis set on all other atoms with the PBE exchange – correlation functional.[46,47] The geometries of **1b** and **2b** were fully optimized starting from the X-ray crystal structure of each complex,[39,48] those for **3b**, **4b**, and **5b** were optimized using the crystal structure of **1b**, geometries for **6b** and **7b** were optimized based on the crystal structure of **7a**,[33] the geometry for **8b** was optimized based on the crystal structure of $[Ru(dqpy)(acac)(CH_3CN)]^{2+}$,[49]

the geometries of **9b** and **10b** were optimized based on the optimized structure of **8b**, the geometry of **11b** was optimized based on the crystal structure of **8a**,[50] and all were verified to have positive harmonic frequencies, confirming the calculated structures as electronic energy minima. Spin densities were calculated using Mulliken population analysis (MPA) methods. Molecular orbitals from the Gaussian calculations were plotted using the Chemcraft program,[51] and the analysis of the molecular orbitals and Mayer bond order calculations in terms of user-defined fragments were performed using AOMix-FO within the AOMix program.[52,53]

Franck–Condon Line-shape Analysis of 77 K Emission. Emission data for **1a** – **11a** and **1b** – **11b** were obtained in a 4:1 (v:v) EtOH/MeOH glass at 77 K and fit to a single-mode Franck–Condon line-shape analysis equation.[16,54] The emission data were obtained as a function of wavelength and converted to energy (cm^{-1}) using a procedure detailed in a previous publication,[55] were then normalized, and were fitted to eq 1 in Wolfram Mathematica 12.2 utilizing the Levenberg – Marquardt method to achieve least–squares error minimization.

$$I(\tilde{\nu}) = \sum_{\nu=0}^{2}\left[\left(\frac{E_{00}-\nu\hbar\omega_M}{E_{00}}\right)^3\left(\frac{S_M^{\nu}}{\nu!}\right)exp\left[-4\ln(2)\left(\frac{(\tilde{\nu}-E_{00}+\nu\hbar\omega_M)}{\Delta\nu_{1/2}}\right)^2\right]\right] \quad (1)$$

In eq 1, $I(\tilde{\nu})$ is the emission intensity as a function of wavenumber, E_{00} is the energy of the transition between the lowest vibrational levels of the ground and excited states, $\hbar\omega_M$ is the weighted-average vibronic acceptor mode observed, ν is the vibronic quantum number in the ground-state acceptor mode, $\Delta\nu_{1/2}$ is the full-width at half-maximum of the vibronic components comprising the emission spectrum, and S_M is the Huang-Rhys factor.

Results and Discussion.

Steady-State Photophysical Properties and Electrochemistry

The electronic absorption spectra of **1b – 11b** in acetone are shown in Figure 2 and their absorption maxima and extinction coefficients are provided alongside those of **1a** – **11a** in Table 1. The ^{1}MLCT absorption maxima of **1b – 11b** are red-shifted as compared to their acetonitrile analogs, as previously reported for a number of Ru–(py) and Ru–(CH_3CN) complexes; this shift is attributed to the relative amount of π-backbonding from the Ru(dπ) t_{2g}-type orbitals to CH_3CN, which is stronger than that to pyridine. For example, the ^{1}MLCT maximum of *cis*–$[Ru(bpy)_2(py)_2]^{2+}$ at 457 nm in dichloromethane shifts to 425 nm in *cis*–$[Ru(bpy)_2(CH_3CN)_2]^{2+}$ in the same solvent, corresponding to an energy difference of 1640 cm^{-1} (0.2 eV).[56] This value is comparable to the shift observed between the two series reported herein. For example, an energy difference of 610 cm^{-1} (0.08 eV) is observed from **1a** to **1b** and 1140 cm^{-1} (0.14 eV) between **6a** and **6b**.

Table 1. Electronic Absorption Maxima, λ_{max}, and Molar Extinction Coefficients, ε, for **1a** – **11a** (L' = CH_3CN) and **1b** – **11b** (L' = py) in Acetone.

Complex	Bidentate Ligand L	**1a** – **11a** (L' = CH_3CN) λ_{max}/nm (ε x10^3 / $cm^{-1}M^{-1}$)[a]	**1b – 11b** (L' = py) λ_{max}/nm (ε x10^3 / $cm^{-1}M^{-1}$)
1	bpy	455 (10.4)	468 (8.1)[b]
2	phen	455 (11.0)	411 (7.7), 467 (9.3)[c]
3	dmb	456 (9.9)	470 (9.1)[d]
4	dmob	458 (8.8), 530 (1.7), 585 (0.7)	474 (8.8), 563 (1.7)
5	dtb	455 (10.4), 515 (1.8), 570 (0.6)	472 (8.0), 551 (1.4)
6	bim	465 (5.4), 545 (1.6), 600 (0.9)	491 (3.4)
7	tmbim	468 (5.7), 555 (1.6), 620 (0.8)	498 (6.5), 592 (1.8), 660 (1.1)
8	acac	530 (5.8)	370 (10), 551 (4.9)[e]
9	Cl-acac	519 (5.5)	369 (12), 537 (6.3)[e]
10	Br-acac	521 (5.4)	371 (13), 539 (6.4)[e]
11	thd	535 (5.9)	373 (13), 551 (6.4)[e]

[a]From ref. 33. [b]From ref. 58. [c]From ref 39. [d]From ref. 38. [e]From ref. 40.

Within each series, it is evident that the electronic absorption maxima of **1b – 11b** shown in Figure 2 mirror those in **1a – 11a** in Figure S7. In both series, a shift of the ^{1}MLCT transition to lower energies is observed from the neutral bpy/phen-type bidentate ligands at ~470 nm in **1b** – **5b**, shifting to lower energy for bim and tmbim at ~500 nm in **6b** and **7b**, followed by complexes with the acac ligand and its derivatives (**8b** – **11b**) at ~550 nm. The moderately intense ^{1}MLCT bands in the 467 – 551 nm range contain contributions from both Ru(dπ) → L(π*) and Ru(dπ) → tpy(π*) transitions. All complexes in the series also display lower energy shoulders at ~540 –650 nm for **1b** – **7b** and ~700 nm for **8b** – **11b** that are Ru(dπ) → tpy(π*) in nature.[57]

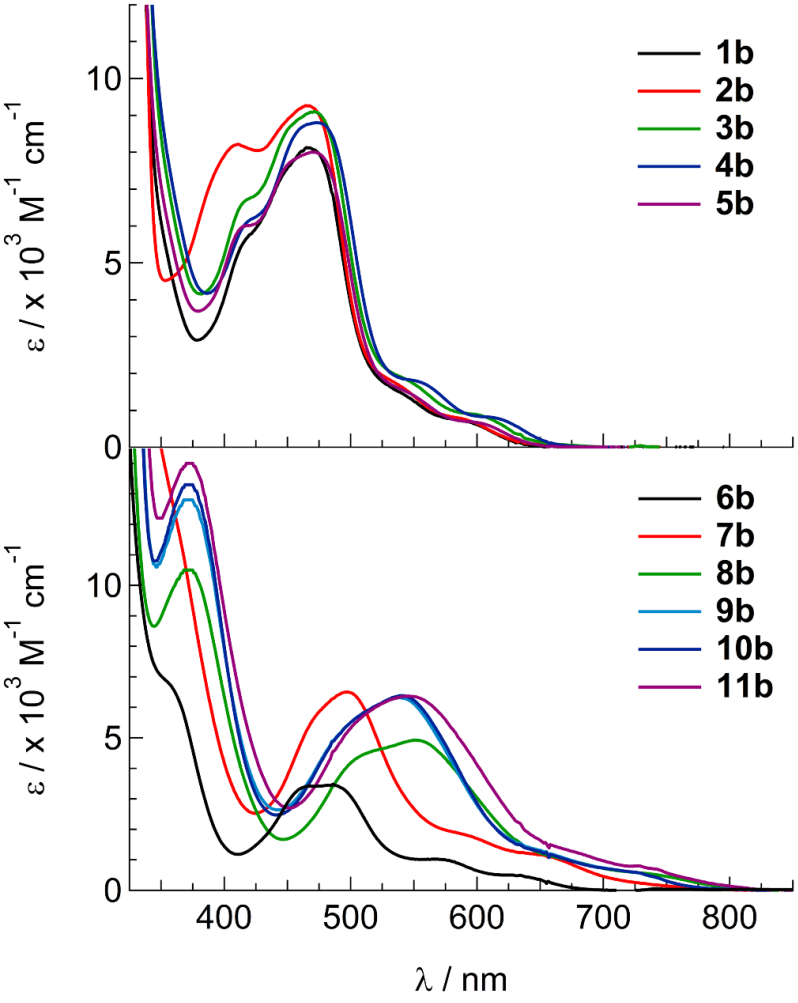

Figure 2. Electronic absorption spectra of **1b** – **5b** (top) and **6b** – **11b** (bottom) in acetone.

The electrochemical reduction potentials for **1a** – **11a** and **1b** – **11b** are listed in Table 2 and examples of cyclic voltammograms for **4b** – **7b** are shown in Figure S8. The first oxidation in **1b** – **11b** is assigned to the reversible $Ru^{III/II}$ redox couple, as is typically observed for Ru(II) polypyridyl complexes.[59] An anodic shift of this couple is recorded as the electron donating ability of the bidentate ligand increases, a trend previously observed in **1a** – **11a**.[35] The reduction in **1b** – **11b** in the –1.14 to –1.48 V (*vs* Ag/AgCl) range is assigned to the reversible reduction of the tpy ligand and compares well to the $tpy^{0/-}$ couples reported for related complexes.[60–62] Across the series, the value of $E_{1/2}(tpy^{0/-})$ shifts by 34 mV, which is of smaller magnitude than that observed for the $Ru^{III/II}$ couple, 71 mV. In each series, the energy gap between the oxidation and reduction potentials, the HOMO–LUMO gap, decreases from **1** to **11** (Table 2), consistent with the bathochromic shift of the electronic absorption spectra within each series (Table 1, Figures 3 and S7). Overall, these data show that the trends in the ground state characteristics of these complexes do not vary significantly with the identity of the monodentate ligand in **1** – **11**.

Table 2. Electrochemical Reduction Potentials for $[Ru(tpy)(L)(L')]^{2+}$ Complexes **1a** – **11a** (L' = CH3CN) and **1b** – **11b** (L' = py) in CH_3CN (0.1 M $TBAPF_6$, *vs* Ag/AgCl).

Complex	Bidentate Ligand L	$E_{1/2}$ / V	
		1a – **11a** (L' = CH_3CN)[a]	**1b – 11b** (L' = py)
1	bpy	+1.33, –1.24	+1.31, –1.23[b]
2	phen	+1.33, –1.26	+1.28, –1.22[c]
3	dmb	+1.29, –1.25	+1.30, –1.14[d]
4	dmob	+1.23, –1.25	+1.16, –1.23
5	dtb	+1.29, –1.24	+1.22, –1.21
6	bim	+1.09, –1.36	+1.03, –1.41
7	tmbim	+1.01, –1.35	+0.90, –1.31
8	acac	+0.70, –1.46	+0.66, –1.43[e]
9	Cl-acac	+0.77, –1.42	+0.70, –1.42[e]
10	Br-acac	+0.78, –1.42	+0.69, –1.42[e]
11	thd	+0.66, –1.50	+0.60, –1.48[e]

[a]From ref. 35. [b]From ref. 48. [c]From ref. 39. [d]From ref. 38. [e]From ref. 40.

Excited State Properties and Photoreactivity

Complexes **1a – 11a** are known to undergo CH_3CN dissociation upon visible light irradiation in H_2O with photoaquation quantum yields, Φ_{450}, that range from 0.0022 to 0.018, increasing with the electron donating ability of the bidentate ligand (λ_{irr} = 450 nm).[33] In a previous publication, **1b** was shown to undergo pyridine ligand exchange with visible light irradiation with very low efficiency, $\Phi_{500} < 0.0001$ in CH_3CN (λ_{irr} = 500 nm),[23] similar to that measured for **4b**, $\Phi_{490} = 6.5 \times 10^{-5}$ in CH_3CN (λ_{irr} = 490 nm).[38] The exchange of the pyridine ligand for a solvent molecule upon visible light irradiation was not detected for **8b** – **11b**, indicating the ligand exchange quantum yield is too low to quantify under our experimental conditions.[40] For complexes **2b** – **7b**, the photoreactivity was either similar to that observed for **1b** or ligand dissociation not observed (Figure S9), such that the quantum yields for the series are estimated to be $\Phi_{500} < 0.0001$ (λ_{irr} = 500 nm). Given that the only chemical difference between the two series is the identity of the monodentate ligand, and following the observed similarities in the ground state properties, it may be concluded that the differences in photochemical reactivity must arise from the excited states of the CH_3CN and pyridine complexes.

Electronic Structure Calculations

To help elucidate the differences in photophysical behavior between these series of complexes, density functional theory (DFT) calculations were performed to characterize the bonding and electronic structures of **1b** – **11b** and compare them to previously published results for the acetonitrile analogs, **1a** – **11a**.[33] Geometry optimizations for the series in the ^{1}GS produced structures that are in good agreement with previously published crystal structures (Tables S1 – S6) and contain no negative harmonic frequencies, confirming the calculated structures as local energy minima. The frontier molecular orbitals calculated for **1b** – **11b** mirror patterns observed for **1a** – **11a**. In both series, the highest occupied molecular orbitals **(**HOMOs) are mostly comprised of Ru d-orbital character with contributions from the bidentate ligand that increase across each series from **1** to **11**.[33] The lowest unoccupied molecular orbitals (LUMOs) of **1b** – **11b** are almost entirely

localized on the tpy ligand, in agreement with the electrochemistry and the results for **1a** – **11a** (Table 2).

It has been shown by the Turro group that in complexes that photodissociate an acetonitrile ligand, the quantum yield of ligand exchange increases as the %Ru d-orbital character in the ^{1}GS HOMO decreases. In contrast, in the analogous pyridine releasing complexes, the ligand exchange quantum yield does not display a clear pattern with respect to %Ru d-orbital character.[33,63] The calculated %Ru d-orbital character in the ^{1}GS HOMOs of **1a** – **11a** and **1b** – **11b** are listed in Table 3. Comparing the two series, these values do not vary significantly with the identity of the monodentate ligand, and the values in **1b** – **11b** decrease as the bidentate ligand becomes more electron withdrawing, mirroring the pattern previously reported for **1a – 11a**. However, unlike **1a – 11a**, the pyridine photodissociation by **1b – 11b** is very low or is not observed (Figure S9).

Table 3. Calculated Mulliken Spin Density in the ^{3}MLCT state and %Ru d character in the ^{1}GS HOMO of $[Ru(tpy)(L)(L')]^{2+}$ Complexes **1a – 11a** (L' = CH_3CN) and **1b – 11b** (L' = py).

		1a – 11a (L' = CH_3CN)[a]		**1b – 11b** (L' = py)	
Complex	Bidentate Ligand L	MSD on Ru in ^{3}MLCT	^{1}GS HOMO %Ru d	MSD on Ru in ^{3}MLCT	^{1}GS HOMO %Ru d
1	bpy	0.881	76.3	0.912	76.6
2	phen	0.878	76.1	0.909	76.6
3	dmb	0.882	76.1	0.912	76.3
4	dmob	0.870	73.2	0.902	74.6
5	dtb	0.886	75.8	0.914	76.4
6	bim	0.882	74.8	0.895	75.8
7	tmbim	0.813	61.2	0.864	64.3
8	acac	0.804	61.3	0.846	62.5
9	Cl-acac	0.741	48.3	0.787	50.9
10	Br-acac	0.738	47.1	0.784	49.9
11	thd	0.786	58.8	0.823	59.8

[a]From ref. 33.

Geometry optimizations and vibrational frequency calculations of **1b** – **11b** were also performed in the lowest energy triplet excited state, ^{3}ES, (Tables S7 – S12), as well as Mulliken spin density (MSD) calculations which have shown to be directly correlated to photophysical behavior.[33,63] In a triplet excited state that is MLCT in nature, the metal center is expected to be in the 3+ oxidation state, such that the spin density on ruthenium would theoretically equal one, since only one unpaired electron is localized in a Ru(dπ) t_{2g}-like orbital and the other on the reduced ligand. In a ^{3}LF state, the spin density on Ru(II) would is expected to equal two, as both unpaired electrons would occupy a metal-center orbital, the Ru(dπ) t_{2g}-like and the Ru(dσ*) e_g-like orbitals. The calculated MSD values for the Ru(II) metal center in the lowest energy ^{3}ESs of **1a – 11a** and **1b – 11b** are listed in Table 2 and confirm the MLCT nature of the lowest energy triplet state. Complexes **1a – 11a** demonstrated an inverse relationship between the MSD on Ru in the ^{3}MLCT state and Φ_{450} for CH_3CN photosubstitution, indicating that ligand exchange became more efficient as the ability of Ru(II) to backbond to CH_3CN decreased.[33] The pyridine series **1b – 11b** mirror the same pattern of MSD values moving across the series. These results demonstrate that the calculated geometric and electronic structures of the two series are similar in the ^{3}MLCT state, therefore, these quantities do not explain the differences in photochemistry.

Franck-Condon Analysis of the ^{3}MLCT Emission

At room temperature, the emission of Ru(II) complexes is typically broad and featureless due to inhomogeneous broadening, but cooling the samples to 77 K results in a hypsochromic shift and reveals vibronic structure that can be modeled to provide ground and excited state information.[10,13,54,64] Franck-Condon (F-C) line-shape analysis was performed on the 77 K luminescence from **1a** – **11a** and **1b** – **11b** in 4:1 EtOH:MeOH (v:v) glasses using a single-mode fit (eq 1), resulting in values of E_{00}, $\hbar\omega_M$, $\Delta\nu_{1/2}$, and the Huang-Rhys factor, S_M, a quantitative measure of the relative distortion in the ^{3}MLCT state as compared to the ^{1}GS, and the resulting optimized parameters are listed in Table 4. Typical fits overlaid with the experimental spectra are shown in Figure 3 for complexes **9a** and **9b**; similar sample fits for complexes **1a**/**b** and **7a**/**b**,

representing complexes containing bpy-type and bim-type ligands, respectively, are available in Figure S10.

Table 4. Franck–Condon Parameters Derived from the Line-Shape Analysis of the 77 K ^{3}MLCT Emission of $[Ru(tpy)(L)(L')]^{2+}$ (L = bidentate ligand) Complexes **1a – 11a** (L' = CH_3CN) and **1b – 11b** (L' = py) in 4:1 EtOH:MeOH (v:v).

	1a – 11a (L' = CH_3CN)				**1b – 11b** (L' = py)			
Complex	E_{00} / cm^{-1}	$\hbar\omega$ / cm^{-1}	S_M	$\Delta\nu_{1/2}$ / cm^{-1}	E_{00} / cm^{-1}	$\hbar\omega$ / cm^{-1}	S_M	$\Delta\nu_{1/2}$ / cm^{-1}
1	16550	1100	0.97	1130	15870	1190	0.76	1115
2	16700	1100	1.00	1150	15950	1290	0.86	1140
3	16270	1080	0.89	1070	15555	1035	0.78	915
4	15860	1050	0.79	1030	15245	895	0.75	905
5	16260	1100	0.93	1100	15590	1020	0.70	970
6	15350	1020	0.68	1020	14730	760	0.53	810
7	14800	970	0.63	990	14145	635	0.43	915
8	13390	1300	0.14	1460	12710	795	0.16	835
9	13840	950	0.43	1050	13180	850	0.19	950
10	13770	900	0.48	920	13200	460	0.50	585
11	13140	940	0.33	840	12590	430	0.12	450

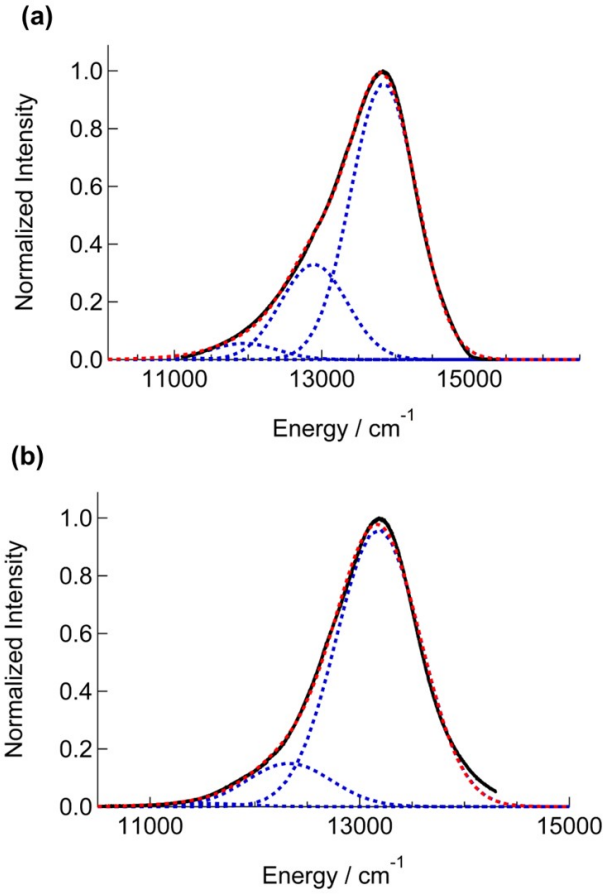

Figure 3. Experimental steady state 77 K emission spectra (solid black line) and single-mode F-C line-shape analysis with individual ^{1}GS acceptor vibrational modes (dashed blue line) and the sum of all calculated ^{1}GS acceptor vibrational modes (dashed red line) of (a) **9a** and (b) **9b**.

The values obtained from the F-C fitting of the 77 K emission provide information about the influence of the mono- and bidentate ligands on the ^{3}MLCT excited states in **1a** – **11a** and **1b** – **11b**. For both series, the energy of the ^{3}MLCT state, E_{00}, decreases moving across the series from **1** to **11** as the electron donating ability of the bidentate ligand increases. This pattern is expected based on π-bonding interactions of the bidentate ligand, which modulate the energy of the t_{2g}-type HOMO. This trend is consistent with the electronic absorption spectra shown in Figures 2 and S7, as well as the decreasing HOMO-LUMO energy gap obtained from electrochemistry measurements (Table 2). In addition, the energies of the ^{3}MLCT states in the

pyridine series are lower than in their acetonitrile analogs, consistent with the decreased π-accepting ability of pyridine as compared to CH_3CN.[63,65]

Values for $\hbar\omega$ greater than ~900 cm^{-1} correspond to vibrations previously observed for the free tpy ligand and for tpy-containing Ru(II) polypyridyl complexes, readily observed in resonance Raman experiments.[66,67] As the electron donating ability increases moving across the series, the average energy of the acceptor mode decreases. This pattern has been observed previously and attributed to increasing contributions from lower frequency vibrations, ~400 cm^{-1}, resulting from variations in the metal-ligand bond lengths.[68–70] This interpretation is consistent with the increased ligand orbital mixing observed in DFT calculations in the ^{3}MLCT states of **1a** – **11a** and **1b** – **11b** (Table 3).

The changes in the Huang-Rhys factor, S_M, in Table 4 show that there is a decrease in the relative distortion between the ^{3}MLCT and ^{1}GS states from **1a** to **11a**, such that greater electron-bidentate ligands with greater electron donating ability result in lower excited state distortion. This pattern is reproduced in the pyridine analogs, **1b – 11b**, though each individual pyridine complex appears to have slightly lower S_M values than the corresponding CH_3CN complex, with the exception of **8b** and **11b**, which have S_M values 0.02 larger than **8a** and **11a**, respectively. The E_{00} values for both series also decrease with increasing electron donating ability of the bidentate ligand, which has been previously observed and expected based on the π-bonding characteristics that affect the energy of the t_{2g}-type HOMO.[54,69] In addition, as E_{00} increases, the mixing between the Ru(dπ) and the bidentate ligand decreases, resulting in a greater degree of charge transfer from the metal/ligand HOMO to the tpy ligand in the ^{3}MLCT state, which can be associated with greater structural change around the Ru(II) center. The Huang-Rhys factor in both series of complexes varies linearly with E_{00}, as shown in the plots of S_M *vs* E_{00} values for **1a – 11a** (Figure 4a) and **1b – 11b** (Figure 4b). Given the fitted F-C parameters follow the same patterns in both series, the differences in the photoinduced ligand exchange of **1a – 11a** as compared to **1b – 11b** cannot be explained through the analysis of the 77 K emission data.

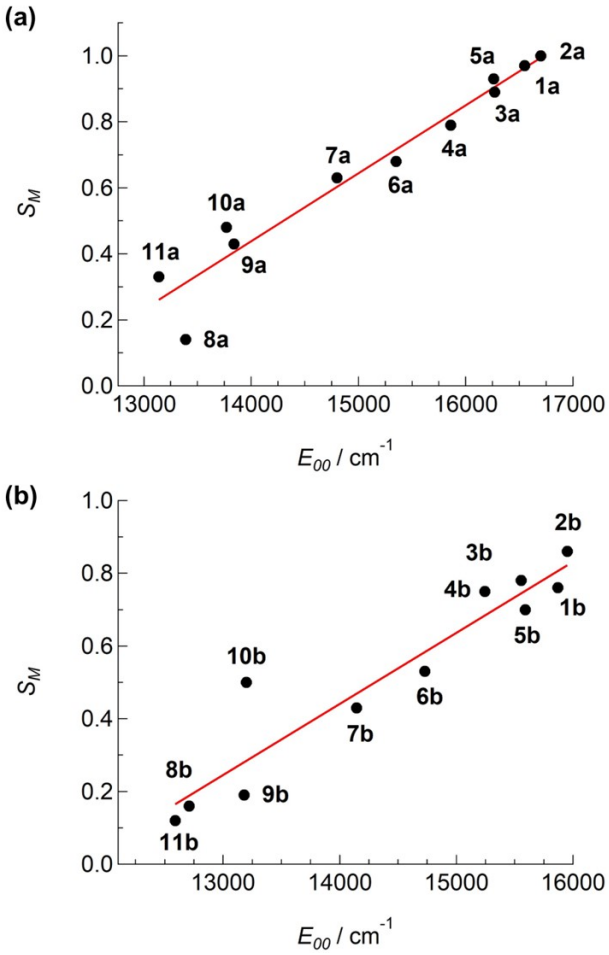

Figure 4. Plot of S_M *vs* E_{00} values for complexes (a) **1a** – **11a** and (b) **1b – 11b**. The data are fit to a linear equation (solid red line) with (a) $R^2 = 0.94$ and (b) $R^2 = 0.90$.

It should be noted that previous series of Ru(II) polypyridyl complexes that demonstrated linear relationship of S_M with E_{00} obey the energy gap law. In contrast, complexes **1a – 11a** have been shown to exhibit opposite energy gap law behavior based on the magnitude of their room temperature ^{3}MLCT decay rate constants, k_{obs}, as a function of E_{00}.[34] As stated above, the energy gap law governs the rate of nonradiative decay, which cannot be measured directly but can be calculated using emission quantum yields, Φ_{em}, observed excited state lifetimes, τ_{obs}, where $k_{obs} = 1/\tau_{obs}$, and the equations $k_r = \Phi_{em} k_{obs}$ and $k_{obs} = k_r + k_{nr}$.[71] Measurements of emission quantum yields for **1a – 11a** and **1b** – **11b** were not successful at room temperature due to the weak emission

from the complexes, such that k_{nr} could not be calculated for either series. To probe the energy gap law behavior in the pyridine series, the room temperature lifetimes of complexes **1b** – **11b** were measured and the results are available in Table S13. A plot of ln(k_{obs}) *vs* E_{00} for both series is shown in Figure 5 and two distinct trends are apparent. For complexes **1a** – **11a**, there is a clear positive slope indicating the observed rates of decay decrease as the energy of the ^{3}MLCT state increases. Complexes **1b** – **5b** display a linear trend similar to the acetonitrile analogs, suggesting that they do not obey the energy gap law. This trend for **1b** – **5b** is not surprising given the observed behavior of **1a** – **11a**, as these complexes do undergo photoinduced substitution of the pyridine ligand, albeit very inefficiently, as shown for complex **1b** and **4b** as described above.[23,38] On the other hand, complexes **6b** – **11b** show a moderate negative slope in ln(k_{obs}) with respect to E_{00}, indicating that these complexes do follow the energy gap law. Interestingly, **6b** – **11b** are also the only 6 of the 22 complexes investigated herein that do not undergo photoinduced ligand exchange, further highlighting how the identity of the monodentate ligand greatly impacts the photophysical behavior in Ru(II)-terpyridine complexes.

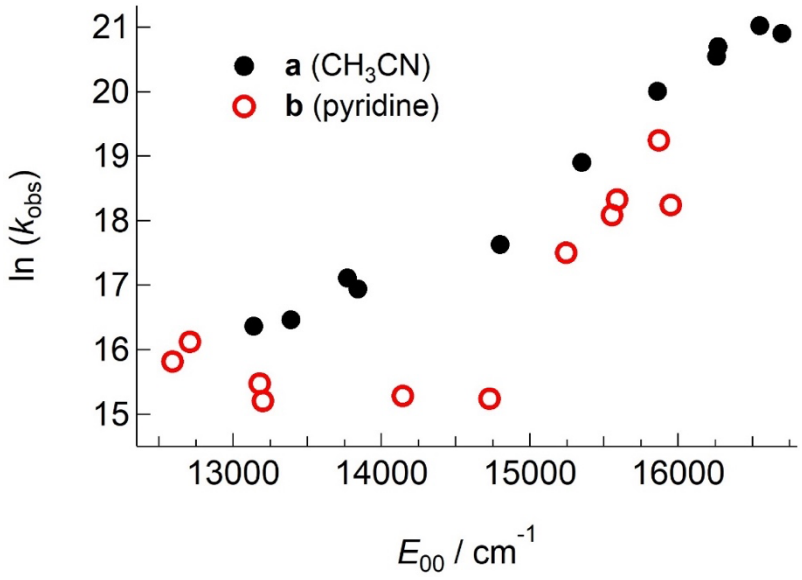

Figure 5. Plot of ln(k_{obs}) vs E_{00} for complexes **1a** – **11a** and **1b** – **11b**.

Activation Barrier between ^{3}MLCT and ^{3}LF States

Arrhenius analysis of the temperature dependence of ^{3}MLCT lifetimes was performed for complexes **1b** – **11b** and compared to previously published data for **1a** – **11a**. The observed rate of decay, k_{obs}, of the ^{3}MLCT state as a function of temperature was fitted according to eq 2,

$$\frac{1}{\tau} = k_{obs} = k_0 + Ae^{\frac{-E_a}{k_B T}} \quad (2)$$

where τ is the observed excited state lifetime, k_0 is a temperature-independent constant corresponding to $k_r + k_{nr}$ over a temperature range, A is the pre-exponential factor, E_a is the activation energy barrier, k_B is Boltzmann's constant, and T is the temperature in K. The data points were allowed to fit with floating variables unless the fit did not converge, in which case the value of k_0 was fixed to an average value from the experimental data at –100 °C to obtain reasonable fitting parameters.

Sample Arrhenius plots of one trial of the data collected for complexes **1b** – **11b** in acetone are presented in Figure 6 along with those previously collected for complexes **3a**, **4a**, and **6a** – **11a** for comparison.[35] Generally, the ^{3}MLCT states in complexes **1b** – **11b** are longer-lived than those of **1a** – **11a**, as shown in Figure 6. The pyridine complexes do not display an exponential increase in k_{obs} until higher temperatures as compared to their acetonitrile analogs, indicative of larger activation barriers. Additionally, the acac-containing complexes **8b** – **11b** exhibit ^{3}MLCT lifetimes that are relatively invariant with respect to temperature across the temperature range investigated. Arrhenius analysis was repeated for complexes **8b** – **11b** in butyronitrile, which has a boiling point of +117 °C as compared to +56 °C for acetone, to expand the temperature range over which data could be collected. However, experiments in butyronitrile did not produce data that could be fit as reliably as the data collected in acetone.

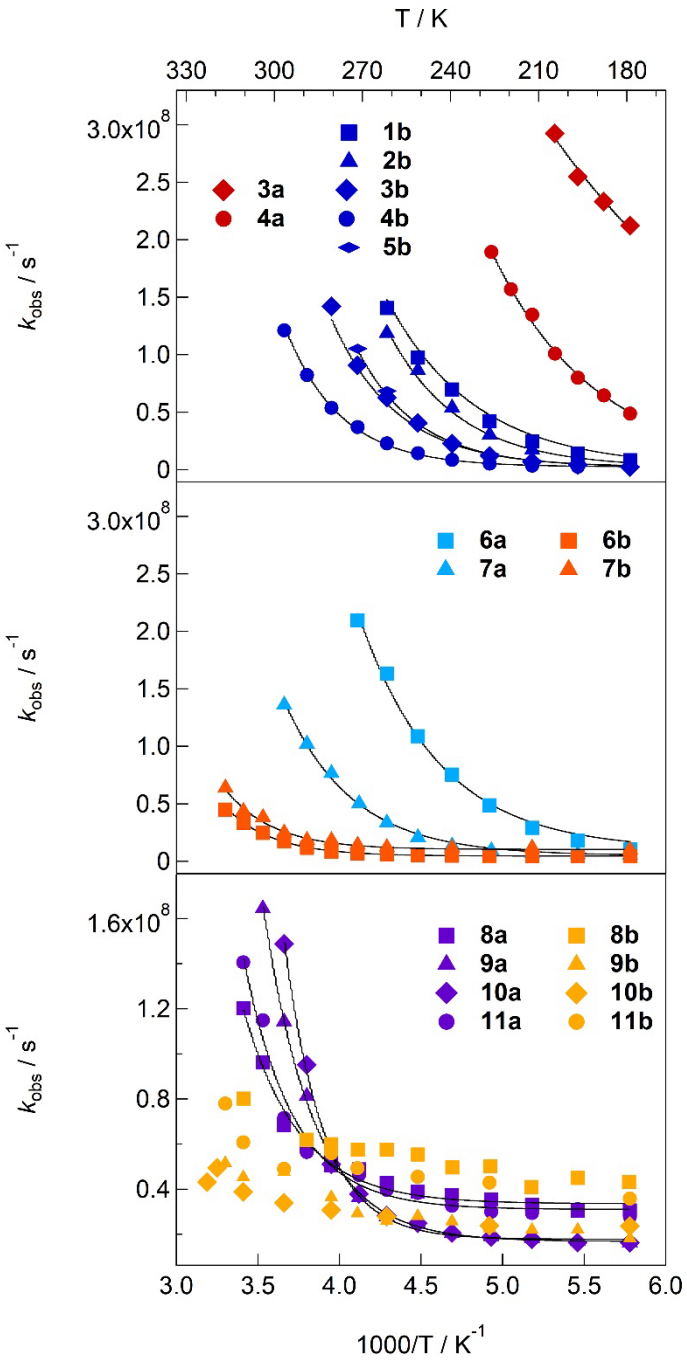

Figure 6. Examples of Arrhenius plots for **3a**, **4a**, **6a** – **11a**, and **1b** – **11b** in acetone. Solid lines represent the best fits to eqn. 2.

Arrhenius parameters obtained from the fits to eq 2 are listed in Table 5 for complexes **1b** – **7b**, alongside those previously published for **3a**, **4a**, and **6a** – **11a**.[35] It is evident from Table 5 that the E_a values in the pyridine series increase with the electron donating ability of the bidentate

ligand, mirroring the pattern observed for the corresponding acetonitrile complexes. Greater E_a values were generally obtained for **1b** – **7b** as compared to their acetonitrile analogs, consistent with the lower energy ^{3}MLCT states in the pyridine series. The relative invariability of k_{obs} in **8b** – **11b** over the temperature range investigated precluded the collection of reliable fitted Arrhenius parameters. Generally, the values of A for the acetonitrile series are on the order of 10^{10} – 10^{12} s^{-1} and those for the pyridine series are 10^{11} - 10^{12} s^{-1}. These values are similar to those reported for bis-tridentate Ru(II) complexes.[72–74]

Table 5. Fitted Arrhenius Parameters from the 77 K Emission of $[Ru(tpy)(L)(L')]^{2+}$ (L = bidentate ligand) Complexes **3a**, **4a**, **6a** – **11a**, and **1b** – **7b** in Acetone.

	3a, **4a**, **6a** – **11a** (L' = CH_3CN)[a]			**1b** – **7b** (L' = py)		
Complex	E_a / cm^{-1}	A / s^{-1}	k_0 / s^{-1}	E_a / cm^{-1}	A / s^{-1}	k_0 / s^{-1}
1	-	-	-	1300 ± 75	4(2) x 10^{11}	2.5 x 10^{6} [b]
2	-	-	-	1610 ± 10	2.49(4) x 10^{12}	2.5 x 10^{6} [b]
3	585 ± 35	2.7(7) x 10^{10}	-	1750 ± 75	3(1) x 10^{12}	2.5 x 10^{6} [b]
4	935 ± 170	2(2) x 10^{11}	-	2060 ± 50	6(2) x 10^{12}	2.4(7) x 10^{6}
5	-	-	-	1880 ± 70	7(3) x 10^{12}	2.5 x 10^{6} [b]
6	1164 ± 134	2(1) x 10^{11}	8 x 10^{6} [b]	2380 ± 70	3(1) x 10^{12}	4.5(2) x 10^{6}
7	1307 ± 273	2(3) x 10^{11}	7 x 10^{6} [b]	2340 ± 170	3(3) x 10^{12}	1.03(8) x 10^{7}
8	1222 ± 287	4(6) x 10^{10}	2.8(7) x 10^{7}	-	-	-
9	1420 ± 175	2(1) x 10^{11}	1.5(3) x 10^{7}	-	-	-
10	1960 ± 340	4(7) x 10^{12}	1.8(5) x 10^{7}	-	-	-
11	1658 ± 228	4(5) x 10^{11}	3.1(4) x 10^{7}	-	-	-

[a]From ref. 75. [b]Values held constant.

It should be noted that while the energies of the ^{3}MLCT states are lower for **1b** – **11b** as compared to those of **1a** – **11a**, the lifetimes of the ^{3}MLCT states of the former are longer, and the energy barriers to populating a ^{3}LF state from the ^{3}MLCT state are higher in the pyridine than in the acetonitrile series. While in complexes **1a** – **11a** the value of Φ_{450} increases with E_a, the ligand

exchange is too low to quantify **1b** – **11b**. In fact, complexes **1b** – **11b** display minimal or no photosubstitution. This difference in photoreactivity is further illustrated when the log of observed rates of excited state decay, k_{obs}, are plotted as a function of E_a (Figure 7). It is apparent that both series follow the same trend, whereby as the energy barrier to populating the ^{3}LF state from the ^{3}MLCT state increases, the observed rate of excited state decay decreases, highlighting the involvement of the ^{3}LF state in excited state decay despite the differences in ligand substitution. Taken together these data indicate that photosubstitution is not occurring from the ^{3}MLCT state in **1b** – **11b**, as is the case in **1a** – **11a**, as this would result in increasing ligand exchange quantum yields moving from **1** to **11** across the series.[35] Instead, the mechanism of ligand exchange in the pyridine series likely involves thermal population of the ^{3}LF state as is typically observed for Ru(II) polypyridyl complexes.[31,32,57,76]

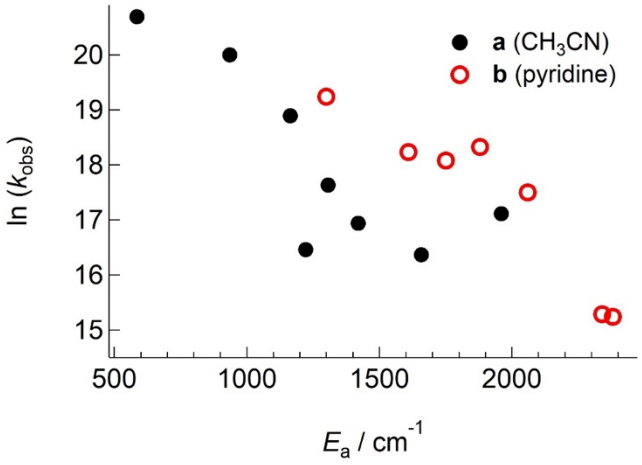

Figure 7. Plot of ln(k_{obs}) vs E_a in complexes **3a**, **4a**, **6a** – **11a**, and **1b** – **7b**.

Conclusion

A series of complexes with the formula $[Ru(tpy)(L)(py)]^{2+}$ **(1b – 11b)**, where L represents a series of 11 bidentate ligands of increasing electron donating character moving from **1** to **11**, was

synthesized as a pyridine analog to the acetonitrile containing series **1a – 11a.** Complexes **1a – 11a** are known to undergo CH_3CN photodissociation upon visible light irradiation and demonstrate anti-energy gap law photophysical behavior. In contrast, complexes **1b** – **11b** display either negligible ligand exchange or do not exchange the pyridine ligand following irradiation. Electronic absorption spectra and cyclic voltammetry demonstrated that the ground states of the two series are similar, indicating that the differences in photoreactivity may originate from variations in the excited states of the two series. DFT calculations on the ^{1}GS and ^{3}MLCT states and Franck-Condon line-shape analysis of 77 K emission further showed the similarities between the two series. F-C analysis of both series followed patterns expected for Ru(II) polypyridyl complex. Investigation into the energy gap law behavior of complexes **1b** – **11b** revealed differences between the two series. Complexes **1b** – **5b** show a similar trend to **1a** – **11a** and undergo ligand exchange, albeit very inefficiently, whereas **6b** – **11b** display photophysical behavior that obeys the energy gap law and do not undergo ligand substitution. Arrhenius analysis of the temperature dependence of ^{3}MLCT state lifetimes showed that the energy barrier to populating the ^{3}LF state from the ^{3}MLCT state increases moving across the series from **1b** to **7b**, similar to the pattern observed for the acetonitrile analogues. However, while ligand exchange quantum yields increased with E_a in the acetonitrile series, the same pattern was not observed in the pyridine series. These findings highlight the impact of the monodentate ligand on the photoreactivity of Ru(II) polypyridyl complexes, with the mechanism of ligand exchange moving from population of the ^{3}MLCT state in **1a** – **11a** to requiring thermal population of a ^{3}LF state in **1b** – **11b**.

Associated Content

Supporting Information. ^{1}H NMR spectra, electronic absorption spectra, electrochemistry, DFT coordinates, example Franck-Condon fits of 77 K emission, and room temperature lifetime data.

Author Information. *Corresponding Author: E-mail: turro.1@osu.edu (C.T.).

Author Contributions: M.N.D. and S.J.S. contributed equally. The manuscript was written through contribution from all authors. All authors have given approval to the final version of the manuscript.

Acknowledgements. The authors thank the National Science Foundation (CHE-2102508) for partial support of this work.

References

(1) van Rixel, V. H. S.; Ramu, V.; Auyeung, A. B.; Beztsinna, N.; Leger, D. Y.; Lameijer, L. N.; Hilt, S. T.; Le Dévédec, S. E.; Yildiz, T.; Betancourt, T.; et al. Photo-Uncaging of a Microtubule-Targeted Rigidin Analogue in Hypoxic Cancer Cells and in a Xenograft Mouse Model. *J. Am. Chem. Soc.* **2019**, *141*, 18444–18454.

(2) Shi, G.; Monro, S.; Hennigar, R.; Colpitts, J.; Fong, J.; Kasimova, K.; Yin, H.; Decoste, R.; Spencer, C.; Chamberlain, L.; et al. Ru(II) Dyads Derived from Alpha-Oligothiophenes : A New Class of Potent and Versatile Photosensitizers for PDT. *Coord. Chem. Rev.* **2015**, *282–283*, 127–138.

(3) Albani, B. A.; Peña, B.; Leed, N. A.; De Paula, N. A. B. G.; Pavani, C.; Baptista, M. S.; Dunbar, K. R.; Turro, C. Marked Improvement in Photoinduced Cell Death by a New Tris-Heteroleptic Complex with Dual Action: Singlet Oxygen Sensitization and Ligand Dissociation. *J. Am. Chem. Soc.* **2014**, *136*, 17095–17101.

(4) Hammarström, L. Accumulative Charge Separation for Solar Fuels Production: Coupling Light-Induced Single Electron Transfer to Multielectron Catalysis. *Acc. Chem. Res.* **2015**, *48* (3), 840–850.

(5) Thompson, D. W.; Ito, A.; Meyer, T. J. $[Ru(bpy)_3]^{2+}$* and Other Remarkable Metal-to-Ligand Charge Transfer (MLCT) Excited States. *Pure Appl. Chem.* **2013**, *85* (7), 1257–1305.

(6) Balzani, V.; Bergamini, G.; Ceroni, P. From the Photochemistry of Coordination Compounds to Light-Powered Nanoscale Devices and Machines. *Coord. Chem. Rev.* **2008**, *252*, 2456–2469.

(7) Bhasikuttan, A. C.; Suzuki, M.; Nakashima, S.; Okada, T. Ultrafast Fluorescence Detection in Tris(2,2′-Bipyridine)Ruthenium(II) Complex in Solution: Relaxation Dynamics Involving Higher Excited States. *J Am Chem Soc* **2002**, *124*, 8398–8405.

(8) Cannizzo, A.; van Mourik, F.; Gawelda, W.; Zgrablic, G.; Bressler, C.; Chergui, M. Broadband Femtosecond Fluorescence Spectroscopy of $[Ru(bpy)_3]^{2+}$. *Angew. Chem. Int. Ed.* **2006**, *45*, 3174–3176.

(9) Juris, A.; Balzani, V.; Barigelletti, F.; Campagna, S.; Belser, P.; Von Zelewsky, A. Ru(II) Polypyridine Complexes: Photophysics, Photochemistry, Electrochemistry, and Chemiluminescence. *Coord. Chem. Rev.* **1988**, *84*, 85–277.

(10) Forster, L. S. Thermal Relaxation in Excited Electronic States of d^3 and d^6 Metal Complexes. *Coord. Chem. Rev.* **2002**, *227*, 59–92.

(11) Wagenknecht, P. S.; Ford, P. C. Metal Centered Ligand Field Excited States: Their Roles in the Design and Performance of Transition Metal Based Photochemical Molecular Devices. *Coord. Chem. Rev.* **2011**, *255*, 591–616.

(12) Sun, Q.; Mosquera-Vazquez, S.; Suffren, Y.; Hankache, J.; Amstutz, N.; Daku, L. M. L.; Vauthey, E.; Hauser, A. On the Role of Ligand-Field States for the Photophysical Properties of Ruthenium(II) Polypyridyl Complexes. *Coord. Chem. Rev.* **2015**, *282–283*, 87–99.

(13) Fleischauer, P. D.; Fleischauer, P. Photoluminescence of Transition Metal Coordination Compounds. *Chem. Rev.* **1970**, *70*, 199–230.

(14) Englman, R.; Jortner, J. The Energy Gap Law for Radiationless Transitions in Large Molecules. *Mol. Phys.* **1970**, *18*, 145–164.

(15) Caspar, J. V; Meyer, T. J. Application of the Energy Gap Law to Nonradiative, Excited-State Decay. *J. Phys. Chem.* **1983**, *87*, 952–957.

(16) Kober, E. M.; Caspar, J. V; Lumpkin, R. S.; Meyer, T. J. Application of the Energy Gap Law to Excited-State Decay of Osmium(II)-Polypyridine Complexes: Calculation of Relative Nonradiative Decay Rates from Emission Spectral Profiles. *J. Phys. Chem.* **1986**, *90*, 3722–3734.

(17) Abrahamsson, M.; Jäger, M.; Kumar, R. J.; Österman, T.; Persson, P.; Becker, H. C.; Johansson, O.; Hammarström, L. Bistridentate Ruthenium(II) Polypyridyl-Type Complexes with Microsecond ^{3}MLCT State Lifetimes: Sensitizers for Rod-like Molecular Arrays. *J. Am. Chem. Soc.* **2008**, *130*, 15533–15542.

(18) Liu, Y.; Hammitt, R.; Lutterman, D. A.; Joyce, L. E.; Thummel, R. P.; Turro, C. Ru(II) Complexes of New Tridentate Ligands: Unexpected High Yield of Sensitized $^1O_2$. *Inorg. Chem.* **2009**, *48*, 375–385.

(19) Foxon, S. P.; Alamiry, M. A. H.; Walker, M. G.; Meijer, A. J. H. M.; Sazanovich, I. V; Weinstein, J. A.; Thomas, J. A. Photophysical Properties and Singlet Oxygen Production by Ruthenium(II) Complexes of Benzo[i]dipyrido[3,2-a :2′,3′-c]phenazine: Spectroscopic and TD-DFT Study. *J. Phys. Chem. A* **2009**, *113*, 12754–12762.

(20) Lifshits, L. M.; Roque III, J. A.; Ramasamy, E.; Thummel, R. P.; Cameron, C. G.; McFarland, S. A. Ruthenium Photosensitizers for NIR PDT Require Lowest-Lying Triplet Intraligand (^{3}IL) Excited States. *J. Photochem. Photobio.l* **2021**, *8*, 100067.

(21) Li, A.; White, J. K.; Arora, K.; Herroon, M. K.; Martin, P. D.; Schlegel, H. B.; Podgorski, I.; Turro, C.; Kodanko, J. J. Selective Release of Aromatic Heterocycles from Ruthenium Tris(2-pyridylmethyl)amine with Visible Light. *Inorg. Chem.* **2016**, *55*, 10–12.

(22) Bonnet, S.; Collin, J.-P.; Sauvage, J.-P.; Schofield, E. Photochemical Expulsion of the Neutral Monodentate Ligand L in Ru(terpy*)(diimine)(L)$^{2+}$: A Dramatic Effect of the Steric Properties of the Spectator Diimine Ligand. *Inorg. Chem.* **2004**, *43*, 8346–8354.

(23) Knoll, J. D.; Albani, B. A.; Durr, C. B.; Turro, C. Unusually Efficient Pyridine Photodissociation from Ru(II) Complexes with Sterically Bulky Bidentate Ancillary Ligands. *J. Phys. Chem. A* **2014**, *118*, 10603–10610.

(24) Havrylyuk, D.; Stevens, K.; Parkin, S.; Glazer, E. C. Toward Optimal Ru(II) Photocages: Balancing Photochemistry, Stability, and Biocompatibility through Fine Tuning of Steric, Electronic, and Physiochemical Features. *Inorg. Chem.* **2020**, *59*, 1006–1013.

(25) Busemann, A.; Flaspohler, I.; Zhou, X. Q.; Schmidt, C.; Goetzfried, S. K.; van Rixel, V. H. S.; Ott, I.; Siegler, M. A.; Bonnet, S. Ruthenium-Based PACT Agents Based on Bisquinoline Chelates: Synthesis, Photochemistry, and Cytotoxicity. *J. Biol. Inorg. Chem.* **2021**, *26*, 667–674.

(26) Arora, K.; Herroon, M.; Al-Afyouni, M. H.; Toupin, N. P.; Rohrabaugh, T. N.; Loftus, L. M.; Podgorski, I.; Turro, C.; Kodanko, J. J. Catch and Release Photosensitizers: Combining Dual-Action Ruthenium Complexes with Protease Inactivation for Targeting Invasive Cancers. *J. Am. Chem. Soc.* **2018**, *140*, 14367–14380.

(27) Respondek, T.; Garner, R. N.; Herroon, M. K.; Podgorski, I.; Turro, C.; Kodanko, J. J. Light Activation of a Cysteine Protease Inhibitor: Caging of a Peptidomimetic Nitrile with $Ru^{II}(bpy)_2$. *J. Am. Chem. Soc.* **2011**, *133*, 17164–17167.

(28) Rohrabaugh, T. N.; Rohrabaugh, A. M.; Kodanko, J. J.; White, J. K.; Turro, C. Photoactivation of Imatinib-Antibody Conjugate Using Low-Energy Visible Light from Ru(II)-Polypyridyl Cages. *Chemical Communications* **2018**, *54*, 5193–5196. https://doi.org/10.1039/c8cc01348a.

(29) Garner, R. N.; Gallucci, J. C.; Dunbar, K. R.; Turro, C. $[Ru(bpy)_2(5\text{-cyanouracil})_2]^{2+}$ as a Potential Light-Activated Dual-Action Therapeutic Agent. *Inorg. Chem.* **2011**, *50*, 9213–9215.

(30) Sharma, R.; Knoll, J. D.; Martin, P. D.; Podgorski, I.; Turro, C.; Kodanko, J. J. Ruthenium Tris(2-pyridylmethyl)amine as an Effective Photocaging Group for Nitriles. *Inorg. Chem.* **2014**, *53*, 3272–3274.

(31) Tfouni, E. Photochemical Reactions of Ammineruthenium(II) Complexes. *Coord. Chem. Rev.* **2000**, *196*, 281–305.

(32) Malouf, G.; Ford, P. C. Photochemistry of the Ruthenium(II) Ammine Complexes, $Ru(NH_3)_5(py\text{-}X)^{2+}$. Variation of Systemic Parameters to Modify Photochemical Reactivities. *J. Am. Chem. Soc.* **1977**, *99*, 7213–7221.

(33) Loftus, L. M.; Al-Afyouni, K. F.; Rohrabaugh, T. N.; Gallucci, J. C.; Moore, C. E.; Rack, J. J.; Turro, C. Unexpected Role of Ru(II) Orbital and Spin Contribution on Photoinduced Ligand Exchange: New Mechanism to Access the Photodynamic Therapy Window. *J. Phys. Chem. C* **2019**, *123*, 10291–10299.

(34) Loftus, L. M.; Rack, J. J.; Turro, C. Photoinduced Ligand Dissociation Follows Reverse Energy Gap Law: Nitrile Photodissociation from Low Energy ^{3}MLCT Excited States. *Chem. Commun.* **2020**, *56*, 4070–4073.

(35) Steinke, S. J.; Piechota, E. J.; Loftus, L. M.; Turro, C. Acetonitrile Ligand Photosubstitution in Ru(II) Complexes Directly from the ^{3}MLCT State. *J. Am. Chem. Soc.* **2022**, *144*, 20177–20182.

(36) Ford, P. C. Properties and Reactions of Ruthenium(II) Amine Complexes. *Coord. Chem. Rev.* **1970**, *5*, 75–99.

(37) N. Storhoff, B.; C. Lewis Jr., H. Organonitrile Complexes of Transition Metals. *Coord. Chem. Rev.* **1977**, *23*, 1–29.

(38) Jang, H. J.; Hopkins, S. L.; Siegler, M. A.; Bonnet, S. Frontier Orbitals of Photosubstitutionally Active Ruthenium Complexes: An Experimental Study of the Spectator Ligands' Electronic Properties Influence on Photoreactivity. *Dalton Trans.* **2017**, *46*, 9969–9980.

(39) Bonnet, S.; Collin, J.-P.; Gruber, N.; Sauvage, J.-P.; Schofield, E. R. Photochemical and Thermal Synthesis and Characterization of Polypyridine Ruthenium(II) Complexes Containing Different Monodentate Ligands. *Dalton Trans.* **2003**, 4654–4662.

(40) Gupta, S.; Vandevord, J. M.; Loftus, L. M.; Toupin, N.; Al-Afyouni, M. H.; Rohrabaugh Jr, T. N.; Turro, C.; Kodanko, J. J. Ru(II)-Based Acetylacetonate Complexes Induce Apoptosis Selectively in Cancer Cells. *Inorg. Chem.* **2021**, *60*, 18964–18974.

(41) Fulmer, G. R.; M Miller, A. J.; Sherden, N. H.; Gottlieb, H. E.; Nudelman, A.; Stoltz, B. M.; Bercaw, J. E.; Goldberg, K. I.; Beckman, M. NMR Chemical Shifts of Trace Impurities: Common Laboratory Solvents, Organics, and Gases in Deuterated Solvents Relevant to the Organometallic Chemist. *Organometallics* **2010**, *29*, 2176–2179.

(42) Pavlishchuk, V. V; Addison, A. W. Conversion Constants for Redox Potentials Measured versus Different Reference Electrodes in Acetonitrile Solutions at 25°C. *Inorg. Chim. Acta* **2000**, *298*, 97–102.

(43) Frisch, M. J. ; Trucks, G. W. ; Schlegel, H. B. ; Scuseria, G. E. ; Robb, M. A. ; Cheeseman, J. R. ; Scalmani, G. ; Barone, V. ; Petersson, G. A. ; Nakatsuji, H. ; et al. *Gaussian 09* **2016**, *revision E*.

(44) Andrae, D.; Häußermann, U.; Dolg, M.; Stoll, H.; Preuß, H. Energy-Adjusted Ab Initio Pseudopotentials for the Second and Third Row Transition Elements. *Theor. Chim. Acta* **1990**, *77*, 123–141.

(45) Schäfer, A.; Horn, H.; Ahlrichs, R. Fully Optimized Contracted Gaussian Basis Sets for Atoms Li to Kr. *J. Chem. Phy.s* **1992**, *97*, 2571–2577.

(46) Perdew, J. P.; Burke, K.; Ernzerhof, M. Generalized Gradient Approximation Made Simple. *Phys. Rev. Lett.* **1996**, *77*, 3865–3868.

(47) Perdew, J. P.; Burke, K.; Ernzerhof, M. Generalized Gradient Approximation Made Simple - ERRATA. *Phys. Rev. Lett.* **1996**, *77*, 1396.

(48) Rasmussen, S. C.; Ronco, S. E.; Mlsna, D. A.; Billadeau, M. A.; Pennington, W. T.; Kolis, J. W.; Petersen, J. D. Ground- and Excited-State Properties of Ruthenium(II) Complexes Containing Tridentate Azine Ligands, Ru(tpy)(bpy)L^{2+}, Where L Is a Polymerizable Acetylene. *Inorg. Chem.* **1995**, *34*, 821–829.

(49) Al-Afyouni, M. H.; Rohrabaugh, T. N.; Al-Afyouni, K. F.; Turro, C. New Ru(II) Photocages Operative with near-IR Light: New Platform for Drug Delivery in the PDT Window. *Chem. Sci.* **2018**, *9*, 6711–6720.

(50) Loftus, L. M.; Al-Afyouni, K. F.; Turro, C. New Ru^{II} Scaffold for Photoinduced Ligand Release with Red Light in the Photodynamic Therapy (PDT) Window. *Chem. Eur. J.* **2018**, *24*, 11550–11553.

(51) Chemcraft; Graphical Software for Visualization of Quantum Chemistry Computations. https://www.chemcraftprog.com. (Last accessed December 22, 2023).

(52) Gorelsky, S. I.; Lever, A. B. P. Electronic Structure and Spectra of Ruthenium Diimine Complexes by Density Functional Theory and INDO/S. Comparison of the Two Methods. *J. Organomet. Chem.* **2001**, *635*, 187–196.

(53) Gorelsky, S. I. AOMix: Program for Molecular Orbital Analysis. https://www.sg-chem.net/aomix/ (Last accessed December 22, 2023)

(54) Motley, T. C.; Troian-Gautier, L.; Brennaman, M. K.; Meyer, G. J. Excited-State Decay Pathways of Tris(bidentate) Cyclometalated Ruthenium(II) Compounds. *Inorg. Chem.* **2017**, *56*, 13579–13592.

(55) Parker, C. A.; Rees, W. T. Correction of Fluorescence Spectra and Measurement of Fluorescence Quantum Efficiency. *Analyst* **1960**, *85*, 587–600.

(56) Sears, R. B.; Joyce, L. E.; Ojaimi, M.; Gallucci, J. C.; Thummel, R. P.; Turro, C. Photoinduced Ligand Exchange and DNA Binding of Cis-[Ru(phpy)(phen)$(CH_3CN)_2]^+$ with Long Wavelength Visible Light. *J Inorg. Biochem.* **2013**, *121*, 77–87.

(57) Hecker, C. R.; Fanwick, P. E.; McMillin, D. R. Evidence for Dissociative Photosubstitution Reactions of $[Ru(trpy)(bpy)(NCCH_3)]^{2+}$. Crystal and Molecular Structure of $[Ru(trpy)(bpy)(py)](PF_6)_2 \bullet (CH_3)_2CO$. *Inorg. Chem.* **1991**, *30*, 659–666.

(58) Knoll, J. D.; Albani, B. A.; Turro, C. Excited State Investigation of a New Ru(II) Complex for Dual Reactivity with Low Energy Light. *Chem. Commun.* **2015**, *51*, 8777–8780.

(59) White, T. A.; Maji, S.; Ott, S. Mechanistic Insights into Electrocatalytic CO_2 Reduction within $[Ru^{II}(tpy)(NN)X]^{n+}$ Architectures. *Dalton Trans.* **2014**, *43*, 15028–15037.

(60) Thummel, R. P.; Chirayil, S. Ruthenium(II) Complexes of Tetra-2-pyridyl-1,4-diazine. *Inorg. Chim. Acta* **1988**, *154*, 77-81.

(61) Constable, E. C.; Cargill Thompson, A. M. W. Pendant-Functionalised Ligands for Metallosupramolecular Assemblies; Ruthenium(II) and Osmium(II) Complexes of 4'-(4-PyridyI)-2,2':6',2"-terpyridine. *J. Chem. Soc. Dalton Trans.* **1994**, 1409-1418.

(62) Tsai, C. N.; Allard, M. M.; Lord, R. L.; Luo, D. W.; Chen, Y. J.; Schlegel, H. B.; Endicott, J. F. Characterization of Low Energy Charge Transfer Transitions in (terpyridine)(bipyridine)Ruthenium(II) Complexes and Their Cyanide-Bridged Bi- and Tri-Metallic Analogues. *Inorg. Chem.* **2011**, *50*, 11965–11977.

(63) Loftus, L. M.; Li, A.; Fillman, K. L.; Martin, P. D.; Kodanko, J. J.; Turro, C. Unusual Role of Excited State Mixing in the Enhancement of Photoinduced Ligand Exchange in Ru(II) Complexes. *J. Am. Chem. Soc.* **2017**, *139*, 18295–18306.

(64) Meyer, T. J. Photochemistry of Metal Coordination Complexes: Metal to Ligand Charge Transfer Excited States. *Pure Appl. Chem.* **1986**, *58*, 1193–1206.

(65) Durham, B.; Walsh, J. L.; Carter, C. L.; Meyer, T. J. Contribution from the Synthetic Applications of Photosubstitution Reactions of Poly(pyridyl) Complexes of Ruthenium(II). *Inorg. Chem.* **1980**, *19*, 860–865.

(66) Schneider, S.; Brehm, G.; Prenzel, C.-J.; Jager, W.; Silva, M. I.; Burrows, H. D.; Formoshinho, S. T. Vibrational Spectra, Normal Coordinate Analysis and Excited-State Lifetimes for a Series of Polypyridylruthenium(II) Complexes. *J. Raman Spectroscopy* **1996**, *27*, 163–175.

(67) Hansen, P. W.; Jensen, P. W. Vibrational Studies on Bis-terpyridine-Ruthenium(II) Complexes. *Spectrochim. Acta A* **1994**, *50*, 169–183.

(68) Caspar, J. V; Meyer, T. J. Photochemistry of MLCT Excited States. Effect of Nonchromophoric Ligand Variations on Photophysical Properties in the Series Cis-$Ru(bpy)_2L_2^{2+}$. *Inorg. Chem.* **1983**, *22*, 2444–2453.

(69) Barqawi, K. R.; Murtaza, Z.; Meyer, T. J. Calculation of Relative Nonradiative Decay Rate Constants from Emission Spectral Profiles. Polypyridyl Complexes of Ru(II). *J. Phys. Chem.* **1991**, *95*, 47–50.

(70) Coe, B. J.; Thompson, D. W.; Culbertson, C. T.; Schoonover, J. R.; Meyer, T. J. Synthesis and Photophysical Properties of Mono(2,2',2"-terpyridine) Complexes of Ruthenium(II). *Inorg. Chem.* **1995**, *34*, 3385–3395.

(71) Wilson, J. S.; Chawdhury, N.; Al-Mandhary, M. R. A.; Younus, M.; Khan, M. S.; Raithby, P. R.; Kohler, A.; Friend, R. H. The Energy Gap Law for Triplet States in Pt-Containing Conjugated Polymers and Monomers. *J. Am. Chem. Soc.* **2001**, *123*, 9412–9417.

(72) Duati, M.; Tasca, S.; Lynch, F. C.; Bohlen, H.; Vos, J. G.; Stagni, S.; Ward, M. D. Enhancement of Luminescence Lifetimes of Mononuclear Ruthenium(II)−Terpyridine Complexes by Manipulation of the σ-Donor Strength of Ligands. *Inorg. Chem.* **2003**, *42*, 8377–8384.

(73) Abrahamsson, M.; Wolpher, H.; Johansson, O.; Larsson, J.; Kritikos, M.; Eriksson, L.; Norrby, P.-O.; Bergquist, J.; Sun, L.; Akermark, B.; et al. A New Strategy for the Improvement of Photophysical Properties in Ruthenium(II) Polypyridyl Complexes. Synthesis and Photophysical and Electrochemical Characterization of Six Mononuclear Ruthenium(II) Bisterpyridine-Type Complexes. *Inorg. Chem.* **2005**, *44*, 3215–3225.

(74) Hammarstrom, L.; Barigelletti, F.; Flamigni, L.; Indelli, M. T.; Armaroli, N.; Calogero, G.; Guardigli, M.; Sour, A.; Collin, J.-P.; Sauvage, J.-P. A Study on Delocalization of MLCT Excited States by Rigid Bridging Ligands in Homometallic Dinuclear Complexes of Ruthenium(II). *J. Phys. Chem. A* **1997**, *101*, 9061–9069.

(75) Steinke, S. J.; Piechota, E. J.; Loftus, L. M.; Turro, C. Acetonitrile Ligand Photosubstitution in Ru(II) Complexes Directly from the ^{3}MLCT State. *J. Am. Chem. Soc.* **2022**, *144*, 20177–20182.

(76) Ford, P. C. The Ligand Field Photosubstitution Reactions of d^6 Hexacoordinate Metal Complexes. *Coord. Chem. Re.v* **1982**, *44*, 61–82.

TOC Graphic

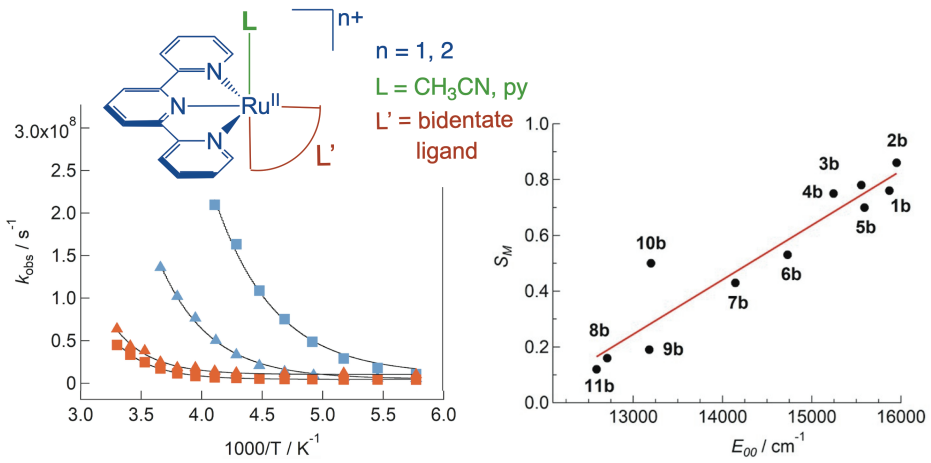
L
n+
n = 1, 2
L = CH3CN, py
L' = bidentate ligand
Ru^II
L'
3.0x10^8
2.5
2.0
1.5
1.0
0.5
0
k_obs / s^-1
3.0
3.5
4.0
4.5
5.0
5.5
6.0
1000/T / K^-1
1.0
0.8
0.6
0.4
0.2
0.0
S_M
2b
3b
4b
1b
5b
10b
6b
7b
8b
9b
11b
13000
14000
15000
16000
E_00 / cm^-1